

ISS: IMAGE AS STEPPING STONE FOR TEXT-GUIDED 3D SHAPE GENERATION

Zhengzhe Liu¹ Peng Dai² Ruihui Li³ Xiaojuan Qi^{2*} Chi-Wing Fu^{1*}

¹The Chinese University of Hong Kong ²The University of Hong Kong ³Hunan University

ABSTRACT

Text-guided 3D shape generation remains challenging due to the absence of large paired text-shape dataset, the substantial semantic gap between these two modalities, and the structural complexity of 3D shapes. This paper presents a new framework called *Image as Stepping Stone* (ISS) for the task by introducing 2D image as a stepping stone to connect the two modalities and to eliminate the need for paired text-shape data. Our key contribution is a *two-stage feature-space-alignment approach* that maps CLIP features to shapes by harnessing a pre-trained single-view reconstruction (SVR) model with multi-view supervisions: first map the CLIP image feature to the detail-rich shape space in the SVR model, then map the CLIP text feature to the shape space and optimize the mapping by encouraging CLIP consistency between the input text and the rendered images. Further, we formulate a *text-guided shape stylization module* to dress up the output shapes with novel structures and textures. Beyond existing works on 3D shape generation from text, our new approach is general for creating shapes in a broad range of categories, *without* requiring paired text-shape data. Experimental results manifest that our approach outperforms the state-of-the-arts and our baselines in terms of *fidelity* and *consistency with text*. Further, our approach can stylize the generated shapes with both realistic and fantasy structures and textures. Codes are available at <https://github.com/liuzhengzhe/ISS-Image-as-Stepping-Stone-for-Text-Guided-3D-Shape-Generation>.

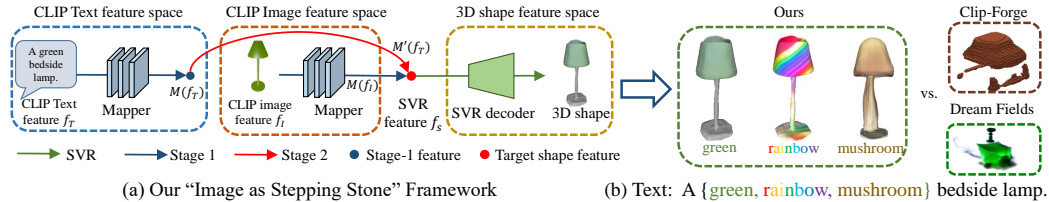


Figure 1: Our novel “Image as Stepping Stone” framework (a) is able to connect the text space (the CLIP Text feature) and the 3D shape space (the SVR feature) through our two-stage feature-space alignment, such that we can generate plausible 3D shapes from text (b) beyond the capabilities of the existing works (CLIP-Forge and Dream Fields), without requiring paired text-shape data.

1 INTRODUCTION

3D shape generation has a broad range of applications, *e.g.*, in Metaverse, CAD, games, animations, etc. Among various ways to generate 3D shapes, a user-friendly approach is to generate shapes from natural language or text descriptions. By this means, users can readily create shapes, *e.g.*, to add/modify objects in VR/AR worlds, to design shapes for 3D printing, etc. Yet, generating shapes from texts is very challenging, due to the lack of large-scale paired text-shape data, the large semantic gap between the text and shape modalities, and the structural complexity of 3D shapes.

Existing works (Chen et al., 2018; Jahan et al., 2021; Liu et al., 2022) typically rely on paired text-shape data for model training. Yet, collecting 3D shapes is already very challenging on its own, let alone the tedious manual annotations needed to construct the text-shape pairs. To our best knowledge, the largest existing paired text-shape dataset (Chen et al., 2018) contains only two categories, *i.e.*, table and chair, thus severely limiting the applicability of the existing works.

Very recently, two annotation-free approaches, CLIP-Forge (Sanghi et al., 2022) and Dream Fields (Jain et al., 2022), were proposed to address the dataset limitation. These two state-of-the-art approaches attempt to utilize the joint text-image embedding from the large-scale pre-trained language vision model, *i.e.*, CLIP (Radford et al., 2021), to eliminate the need of requiring paired text-shape data in model training. However, it is still extremely challenging to generate 3D shapes from text without paired texts and shapes for the following reasons. First, the range of object categories that can be generated are still limited due to the scarcity of 3D datasets. For example, Clip-Forge (Sanghi et al., 2022) is built upon a shape auto-encoder; it can hardly generate plausible shapes beyond the ShapeNet categories. Also, it is challenging to learn 3D prior of the desired shape from texts. For instance, Dream Field (Jain et al., 2022) cannot generate 3D shapes like our approach due to the lack of 3D prior, as it is trained to produce only multi-view images with a neural radiance field. Further, with over an hour of optimization for each shape instance from scratch, there is still no guarantee that the multi-view consistency constraint of Dream Field (Jain et al., 2022) can enforce the model for producing shapes that match the given text; we will provide further investigation in our experiments. Last, the visual quality of the generated shapes are far from satisfactory due to the substantial semantic gap between the unpaired texts and shapes. As shown in Figure 1 (b), the results generated by Dream Field typically look surrealistic (rather than real), due to insufficient information extracted from text for the shape structures and details. On the other hand, CLIP-Forge (Sanghi et al., 2022) is highly restricted by the limited 64^3 resolution and it lacks colors and textures, further manifesting the difficulty of generating 3D shapes from unpaired text-shape data.

Going beyond the existing works, we propose a new approach to 3D shape generation from text without needing paired text-shape data. Our key idea is to *implicitly leverage 2D image* as a stepping stone (ISS) to connect the text and shape modalities. Specifically, we employ the joint text-image embedding in CLIP and train a CLIP2Shape mapper to *map the CLIP image features to a pre-trained detail-rich 3D shape space with multi-view supervisions*; see Figure 1 (a): stage 1. Thanks to the joint text-image embedding from CLIP, our trained mapper is able to connect the CLIP text features with the shape space for text-guided 3D shape generation. Yet, due to the gap between the CLIP text and CLIP image features, the mapped text feature may not align well with the destination shape feature; see the empirical analysis in Section 3.2. Hence, we further fine-tune the mapper specific to each text input by *encouraging CLIP consistency* between the rendered images and the input text to enhance the consistency between the input text and the generated shape; see Figure 1 (a): stage 2.

Our new approach advances the frontier of 3D shape generation from text in the following aspects. First, by taking image as a stepping stone, we make the challenging text-guided 3D shape generation task more approachable and cast it as a single-view reconstruction (SVR) task. Having said that, we learn 3D shape priors from the adopted SVR model directly in the feature space. Second, benefiting from the learned 3D priors from the SVR model and the joint text-image embeddings, our approach can produce 3D shapes in only 85 seconds vs. 72 minutes of Dream Fields (Jain et al., 2022). More importantly, our approach is able to produce plausible 3D shapes, *not* multi-view images, beyond the generation capabilities of the state-of-the-art approaches; see Figure 1 (b).

With our two-stage feature-space alignment, we already can generate shapes with good fidelity from texts. To further enrich the generated shapes with vivid textures and structures beyond the generative space of the pre-trained SVR model, we additionally design a text-guided stylization module to generate novel textures and shapes by encouraging consistency between the rendered images and the text description of the target style. We then can effectively fuse with the two-stage feature-space alignment to enable the generation of both realistic and fantasy textures and also shapes beyond the generation capability of the SVR model; see Figure 1 (b) for examples. Furthermore, our approach is compatible with different SVR models (Niemeyer et al., 2020; Alwala et al., 2022). For example, we can adopt SS3D (Alwala et al., 2022) to generate shapes from single-view in-the-wild images to broaden the range of categorical 3D shapes that our approach can generate, going beyond Sanghi et al. (2022), which can only generate 13 categories of ShapeNet. Besides, our approach can also work with the very recent approach GET3D (Gao et al., 2022) to generate high-quality 3D shapes from text; see our results in Section 10.

2 RELATED WORKS

Text-guided image generation. Existing text-guided image generation approaches can be roughly cast into two branches: (i) direct image synthesis (Reed et al., 2016a;b; Zhang et al., 2017; 2018;

Xu et al., 2018; Li et al., 2019; 2020; Qiao et al., 2019; Wang et al., 2021) and (ii) image generation with a pre-trained GAN (Stap et al., 2020; Yuan & Peng, 2019; Souza et al., 2020; Wang et al., 2020; Rombach et al., 2020; Patashnik et al., 2021; Xia et al., 2021). Yet, the above works can only generate images for limited categories. To address this issue, some recent works explore zero-shot text-guided image generation (Ramesh et al., 2021; Ding et al., 2021; Nichol et al., 2021; Liu et al., 2021; Ramesh et al., 2022) to learn to produce images of any category. Recently, Zhou et al. (2022) and Wang et al. (2022b) leverage CLIP for text-free text-to-image generation. Text-guided shape generation is more challenging compared with text-to-image generation. First, it is far more labor-intensive and difficult to prepare a large amount of paired text-shape data than paired text-image data, which can be collected from the Internet on a large scale. Second, the text-to-shape task requires one to predict full 3D structures that should be plausible geometrically and consistently in all views, beyond the needs in single-view image generation. Third, 3D shapes may exhibit more complex spatial structures and topology, beyond regular grid-based 2D images.

Text-guided 3D generation. To generate shapes from text, several works (Chen et al., 2018; Jahan et al., 2021; Liu et al., 2022) rely on paired text-shape data for training. To avoid paired text-shape data, two very recent works, CLIP-Forge (Sanghi et al., 2022) and Dream Fields (Jain et al., 2022), attempt to leverage the large-scale pre-trained vision-language model CLIP. Yet, they still suffer from various limitations, as discussed in the third paragraph of Section 1. Besides 3D shape generation, some recent works utilize CLIP to manipulate a shape or NeRF with text (Michel et al., 2022; Jetchev, 2021; Wang et al., 2022a) and to generate 3D avatars (Hong et al., 2022). In this work, we present a new framework for generating 3D shape from text without paired text-shape data by our novel two-stage feature-space alignment. Our experimental results demonstrate the superiority of this work beyond the existing ones in terms of fidelity and text-shape consistency.

Single-view reconstruction. Another topic related to this work is single-view reconstruction (SVR). Recently, researchers have explored SVR with meshes (Agarwal & Gopi, 2020), voxels (Zubić & Liò, 2021), and 3D shapes (Niemeyer et al., 2020). Further, to extend SVR to in-the-wild categories, Alwala et al. (2022) propose SS3D to learn 3D shape reconstruction using single-view images in hundreds of categories. In our work, we propose to harness an SVR model to map images to shapes, such that we can take 2D image as a stepping stone for producing shapes from texts. Yet, we perform the mapping and feature alignment implicitly in the latent space rather than explicitly.

3 METHODOLOGY

3.1 OVERVIEW

This work aims to generate 3D shape S from text T . Overall, our idea is to map the CLIP features to the shape space of a pre-trained SVR model, such that we can leverage the joint text-image embeddings from CLIP and also the 3D generation capability of the SVR model to enhance the generation of 3D shape from text. Hence, our method only needs to be trained with multi-view RGB or RGBD images and the associated camera poses without paired text-shape data. As Figure 2 shows, our framework includes (i) image encoder E_S , which maps input image I to SVR shape space Ω_S , (ii) pre-trained CLIP text and image encoders E_T and E_I , which map text T and image I to CLIP spaces Ω_T and Ω_I , respectively, (iii) mapper M with 12 fully-connected layers, each followed by a Leaky-ReLU, and (iv) decoder D to generate the final shape S . Specifically, we use DVR (Niemeyer et al., 2020) as the SVR model when presenting our method, unless otherwise specified.

Overall, we introduce a novel two-stage feature-space-alignment approach to connect the text, image, and shape modalities. In detail, we first train CLIP2Shape mapper M to connect the CLIP image space Ω_I and the shape space Ω_S from the pre-trained SVR model (see Figure 2 (a)). Then, we fine-tune M at test time using a CLIP consistency loss L_c to further connect the CLIP text space Ω_T with Ω_S (see Figure 2 (b)). Last, we may further optimize the texture and structure style of S by fine-tuning the decoders (see Figure 2 (c)).

In the following, we first introduce two empirical studies on the CLIP feature space in Section 3.2, then present our two-stage feature-space-alignment approach in Section 3.3. Further, Section 9 presents our text-guided shape stylization method and Section 3.5 discusses the compatibility of our approach with different SVR models and our extension to generate a broad range of categories.

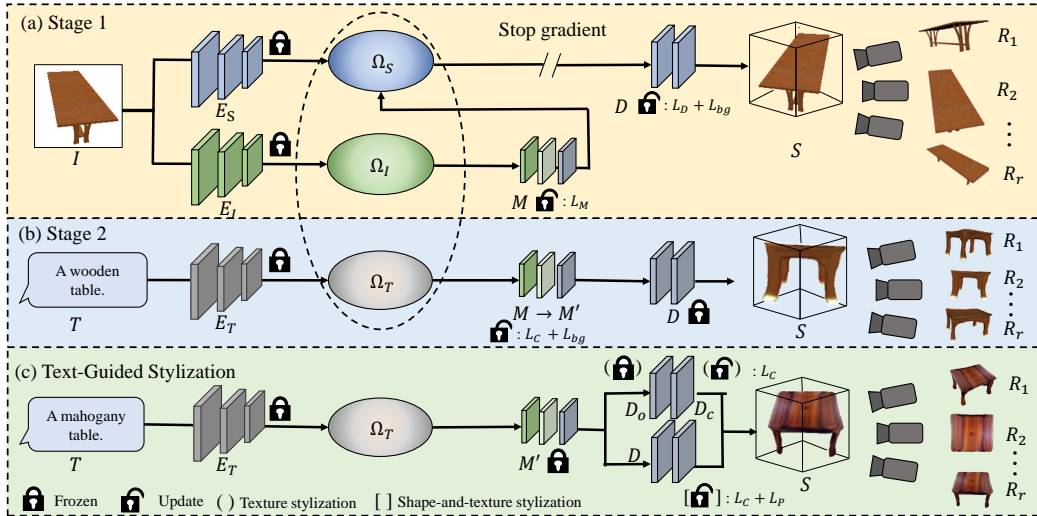


Figure 2: Overview of our text-guided 3D shape generation framework, which has three major stages. (a) Leveraging a pre-trained SVR model, in stage-1 feature-space alignment, we train the CLIP2Shape mapper M to map the CLIP image feature space Ω_I to shape space Ω_S of the SVR model with E_S , E_I frozen, and fine-tune decoder D with an additional background loss L_{bg} . M and D are trained with their own losses separately at the same time by stopping the gradients from SVR loss L_D and background loss L_{bg} to propagate to M . (b) In stage-2 feature-space alignment, we fix D and fine-tune M into M' by encouraging CLIP consistency between input text T and the rendered images at test time. (c) Last, we optimize the style of the generated shape and texture of S for T . At the inference, we use stage 2 to generate 3D shape from T and (c) is optional.

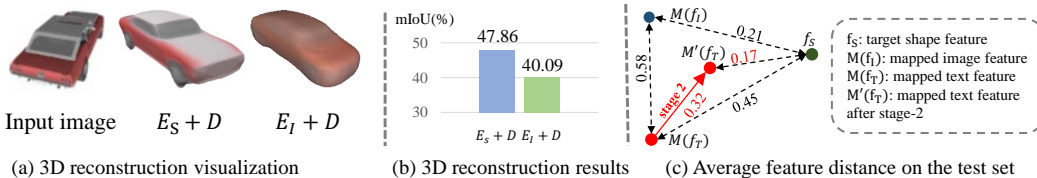


Figure 3: Empirical studies on the CLIP feature space for text-guided 3D shape generation.

3.2 EMPIRICAL STUDIES AND MOTIVATIONS

Existing works (Sanghi et al., 2022; Zhou et al., 2022; Wang et al., 2022b) mostly utilize CLIP directly without analyzing how it works and discussing its limitations. To start, we investigate the merits and drawbacks of leveraging CLIP for text-guided 3D shape generation by conducting the following two empirical studies to gain more insight into the CLIP feature space.

3.2.1 WHETHER CLIP FEATURE SPACE SUFFICIENTLY GOOD FOR 3D SHAPE GENERATION?

First, we study the representative capability of the CLIP image feature space Ω_I by trying to generate 3D shapes from this space. Specifically, we replace the SVR image encoder E_S with the CLIP image encoder E_I , and optimize implicit decoder D using multi-view losses like DVR (Niemeyer et al., 2020) with E_I frozen. This approach can be extended to text-to-shape generation by replacing E_I with CLIP text encoder E_T during the inference. To compare the performance of E_S and E_I , we evaluate 3D mIoU between their generated shapes and GTs. The results are as follows: the standard SVR pipeline $E_S + D$ achieves 47.86% mIoU while replacing the SVR encoder E_S with CLIP encoder E_I ($E_I + D$) degrades the performance to 40.09%. From the results and qualitative comparison shown in Figures 3 (a, b), we can see that the CLIP image space Ω_I has *inferior representative capability to capture details of the input image* for 3D shape generation. This is not surprising, since the pre-trained E_I from CLIP is targeted to extract semantic-aligned features from texts rather than extracting details from images. Hence, image details relevant to 3D reconstruction are lost, e.g., textures. On the contrary, E_S from the SVR model is optimized for 3D generation from images, so it maintains more

necessary details. The above result motivates us to design a mapper M from Ω_I to Ω_S and then generate shapes from Ω_S instead of Ω_I for better generative fidelity.

3.2.2 HOW THE CLIP IMAGE AND TEXT FEATURE GAP INFLUENCES 3D SHAPE GENERATION?

Second, we investigate the gap between the normalized CLIP image feature $f_I \in \Omega_I$ and normalized CLIP text feature $f_T \in \Omega_T$; (see also the CLIP image and text feature spaces in Figure 1 (a)) and how such gap influences text-guided 3D shape generation. Specifically, we randomly sample 300 text-shape pairs from the text-shape dataset (Chen et al., 2018), then evaluate the cosine distance between f_I and f_T , *i.e.*, $d = 1 - \text{cosine_similarity}(f_I, f_T)$, where f_I is the CLIP feature of the rendered images from the corresponding shape. We repeat the experiment and obtain $d(f_T, f_I) = 0.783 \pm 0.004$. The result reveals *a certain gap between the CLIP text and image features in this dataset, even though they are paired*. Also, the angle in the feature space between the two features is around $\arccos(1 - 0.783) = 1.35$ rad in this dataset (Chen et al., 2018). Having said that, directly replacing f_I with f_T like Sanghi et al. (2022); Zhou et al. (2022) in inference may harm the consistency between the output shape and the input text. Taking Figure 1 as an example, directly replacing f_I with f_T causes a cosine distance of 0.59 to $f_S \in \Omega_S$ (see Figure 3 (c)), which is significantly larger than the distance between f_I and f_S (0.12). Our finding is consistent with the findings in Liang et al. (2022). It motivates us to further fine-tune M into M' at test time, such that we can produce feature $M'(f_T)$, which is closer to f_S than $M(f_T)$.

3.3 TWO-STAGE FEATURE-SPACE ALIGNMENT

Following the above findings, we propose a two-stage feature-space-alignment approach to first connect image space Ω_I and shape space Ω_S and further connect text space Ω_T to shape space Ω_S with the image space Ω_I as the stepping stone.

Stage-1 alignment: CLIP image-to-shape mapping. Given multi-view RGB or RGBD images for training, the stage-1 alignment is illustrated in Figure 2 (a). Considering that shape space Ω_S contains richer object details than the image space Ω_I , while Ω_I provides a joint text-image embedding with the input text space Ω_T , we introduce a fully-connected CLIP2Shape mapper M to map image feature f_I to shape space Ω_S . Taking a rendered image I as input, M is optimized with an L_2 regression between $M(f_I)$ and standard SVR feature $f_S = E_S(I)$ according to Equation (1) below:

$$L_M = \sum_{i=1}^N \|M(f_{I,i}) - E_S(I_i)\|_2^2 \quad (1)$$

where N is the number of images in the training set and $f_{I,i}$ is the normalized CLIP feature of I_i .

Also, we fine-tune decoder D to encourage it to predict a white background, which helps the model to ignore the background and extract object-centric feature (see Figure 4), while maintaining its 3D shape generation capability. To this end, we propose a new background loss L_{bg} in Equation (2) below to enhance the model’s foreground object awareness to prepare for the second-stage alignment.

$$L_{bg} = \sum_p \|D_c(p) - 1\|_2^2 \mathbb{1}(\text{ray}(o, p) \cap F = \emptyset) \quad (2)$$

where $\mathbb{1}$ is the indicator function; $F = \{p : D_o(p) > t\}$ indicates the foreground region, in which the occupancy prediction $D_o(p)$ is larger than threshold t ; p is a query point; $\text{ray}(o, p) \cap F = \emptyset$ means the ray from camera center o through p does not intersect the foreground object marked by F ; and $D_c(p)$ is the color prediction at query point p . In a word, L_{bg} encourages D to predict the background region as white color (value 1), such that E_I can focus on and better capture the foreground object. In addition, to preserve the 3D shape generation capability of D , we follow the loss L_D , with which D has been optimized in the SVR training. In this work, we adopt Niemeyer et al. (2020).

Hence, the overall loss in stage-1 training is $\lambda_M L_M$ for mapper M and $\lambda_{bg} L_{bg} + L_D$ for decoder D , where λ_M and λ_{bg} are weights. The stage-1 alignment provides a good initialization for the test-time optimization of stage 2.

Stage-2 alignment: text-to-shape optimization. Given a piece of text, the stage-2 alignment aims to further connect the text and shape modalities. Specifically, it searches for shape S that best matches

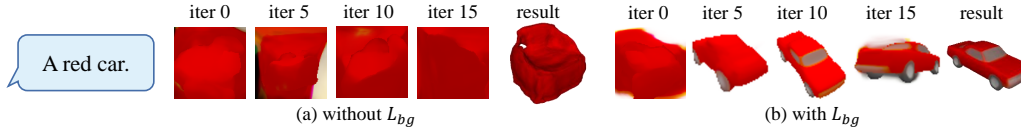


Figure 4: Effect of generating shapes from the same text with/without background loss L_{bg} .

the input text T . To this end, we formulate a fast test-time optimization to reduce the gap between the text and image CLIP features f_T and f_I , as discussed earlier in the second empirical study.

As shown in Figure 2 (b), given input text T , we replace image encoder E_I with text encoder E_T to extract CLIP text feature f_T , then fine-tune M with CLIP consistency loss between input text T and m images $\{R_i\}_{i=1}^m$ rendered with random camera poses from output shape S ; see Equation 3:

$$L_C = \sum_{i=1}^m \langle f_T \cdot \frac{E_I(R_i)}{\|E_I(R_i)\|} \rangle \quad (3)$$

where $\langle \cdot \rangle$ indicates the inner-product.

In stage-2 alignment, we still adopt L_{bg} to enhance the model’s foreground awareness. Comparing Figures 4 (a) and (b), we can see that the stage-2 alignment is able to find a rough shape with L_{bg} in around five iterations, yet failing to produce a reasonable output without L_{bg} , since having the same color prediction on both foreground and background hinders the object awareness of the model.

Thanks to the joint text-image embedding of CLIP, the gap between text feature f_T and shape feature f_S has already been largely narrowed by M . Therefore, the stage-2 alignment only needs to fine-tune M with 20 iterations using the input text, taking only around 85 seconds on a single GeForce RTX 3090 Ti, compared with 72 minutes taken by Dream Fields (Jain et al., 2022) at test time. After this fine-tuning, we can readily obtain a plausible result; see, *e.g.*, the “result” shown in Figure 4 (b). Our ISS is a novel and efficient approach for 3D shape generation from text.

Diversified generation. In general, shape generation from text is one-to-many. Hence, we further extend our approach with diversified 3D shape generation from the same piece of input text. Unlike the existing works, which require additional and complex modules, *e.g.*, GANs (Chen et al., 2018), IMLE (Liu et al., 2022), and normalizing flow network (Sanghi et al., 2022), we can simply perturb the image and text features for diversified generation. Specifically, after stage-1 alignment, we randomly permute f_I as an initialization and f_T as the ground truth by adding normalized Gaussian noises $z_1 = h_1/\|h_1\|$, $z_2 = h_2/\|h_2\|$, where $h_1, h_2 \sim N(0, 1)$ to derive diversified features

$$\hat{f}_I = \tau_1 f_I + (1 - \tau_1) z_1 \quad \text{and} \quad \hat{f}_T = \tau_2 f_T + (1 - \tau_2) z_2, \quad (4)$$

where τ_1, τ_2 are hyperparameters to control the degrees of permutation. With permuted \hat{f}_I and \hat{f}_T in stage-2 alignment, our model can converge to different 3D shapes for different noise.

3.4 TEXT-GUIDED STYLIZATION

The two-stage feature-space alignment is already able to generate plausible 3D shapes; see, *e.g.*, Figures 2 (b) and 4 (b). However, the generative space is limited by the representation capability of the employed SVR model, *e.g.*, DVR (Niemeyer et al., 2020) can only generate shapes with limited synthetic patterns as those in ShapeNet. However, a richer and wider range of structures and textures are highly desired. To this end, we equip our model with a text-guided stylization module to enhance the generated shapes with novel structure and texture appearances, as shown in Figures 2 (c) and 1.

Specifically, for texture stylization, we first duplicate D (except for the output layer) to be D_o and D_c , then put the output occupancy prediction layer and color prediction layer on top of D_o and D_c , respectively. Further, we fine-tune D_c with the same CLIP consistency loss as in Equation (3), encouraging the consistency between input text T and the m rendered images $\{R_i\}_{i=1}^m$.

Besides textures, novel structures are also desirable for shape stylization. Hence, we further incorporate a shape-and-texture stylization strategy to create novel structures. To enable shape sculpting, we fine-tune D with the same CLIP consistency loss in Equation 3. At the same time, to maintain the

overall structure of the initial shape S , we propose a 3D prior loss L_P shown in Equation (5), aiming at preserving the 3D shape prior learned by the two-stage feature-space alignment.

$$L_P = \sum_p |D_o(p) - D'_o(p)| \quad (5)$$

where p is the query point, and D_o, D'_o are the occupancy predictions of the initial D and the fine-tuned D in the stylization process, respectively. To improve the consistency between the generated texture and the generated shape, we augment the background color of R_i with a random RGB value in each iteration. Please find more details in the supplementary material.

3.5 COMPATIBILITY WITH DIFFERENT SVR MODELS

Besides DVR (Niemeyer et al., 2020), our ISS framework is compatible with different SVR models. For example, we can adapt it with the most recent SVR approach SS3D (Alwala et al., 2022) that leverages in-the-wild single images for 3D generation. With this model, our framework can generate a wider range of shape categories by using SS3D’s encoder and decoder as shape encoder E_S and decoder D in our framework, respectively. Here, we simply follow the same pipeline as in Figure 2 to derive a text-guided shape generation model for the in-the-wild categories; see our results in Section 4.4. Notably, we follow the losses in Alwala et al. (2022) in place of L_D (see Section 3.3) in stage-1 training, requiring only single-view images without camera poses. More importantly, our approach’s high compatibility suggests that it is orthogonal to SVR, so its performance can potentially be further upgraded with more advanced SVR approaches in the future.

4 EXPERIMENTS

4.1 DATASETS, IMPLEMENTATION DETAILS, AND METRICS

With multi-view RGB or RGBD images and camera poses, we can train ISS on the synthetic dataset ShapeNet (Chang et al., 2015) (13 categories) and the real-world dataset CO3D (Reizenstein et al., 2021) (50 categories). To evaluate our generative performance, we create a text description set with four texts per category on ShapeNet and two texts per category on CO3D. SS3D (Alwala et al., 2022) takes single-view in-the-wild images in training; as their data has not been released, we only evaluate our method on some of their categories. To evaluate the performance, we employ Fréchet Inception Distance (FID) (Heusel et al., 2017), Fréchet Point Distance (FPD) (Liu et al., 2022) to measure shape generation quality, and conduct a human perceptual evaluation to further assess text-shape consistency. Please refer to the supplementary material for more details on the metrics and implementation details.

4.2 COMPARISONS WITH STATE-OF-THE-ART METHODS

We compare our approach with existing works (Sanghi et al., 2022; Jain et al., 2022) both qualitatively and quantitatively. For a fair comparison, we use their official codes on GitHub to generate shapes on our text set. Table 1 shows quantitative comparisons, whereas Figure 5 shows the qualitative comparisons. Comparing existing works and ours in Table 1, we can see that our approach outperforms two state-of-the-art works by a large margin for both generative quality and text-shape consistency scores. On the other hand, the qualitative comparisons in Figure 5 (a,b) show that CLIP-Forge (Sanghi et al., 2022) produces low-resolution shapes without texture, and some generated shapes are inconsistent with the input text, *e.g.*, “a wooden boat.” Dream Fields (Jain et al., 2022) cannot generate reasonable shapes from the input text on the top row and its generated shape on the bottom row is also inconsistent with the associated input text. On the contrary, our approach (Figure 5 (i)) can generate high-fidelity shapes that better match the input text. Note that we only utilize two-stage feature-space alignment without stylization in producing our results. Please refer to the supplementary file for more results and visual comparisons.

4.3 ABLATION STUDIES

To manifest the effectiveness of our approach, we conduct ablation studies on the following baselines (see Table 1 and Figure 5): generate shapes from $\Omega_I (E_I + D)$, optimize stage-2 alignment without stage-1 (w/o stage 1), conduct stage-1 alignment without stage-2 (w/o stage 2), disable the background loss in stage 1, stage 2 and both (w/o L_{bg_1} , w/o L_{bg_2} , w/o L_{bg}), and two additional baselines that first create images and then 3D shapes (GLIDE+DVR, LAFITE+DVR). More details on the setup and analysis are provided in the supplementary material Section 3. Our results outperforms all the existing works and baselines in terms of fidelity and text-shape consistency by a large margin.

Table 1: Quantitative comparisons with existing works and baselines.

Method Type	Method	FID (\downarrow)	Consistency Score (%) (\uparrow)	FPD (\downarrow)	A/B/C Test
Existing works	CLIP-Forge	162.87	41.83 ± 17.62	37.43	8.90 ± 4.12
	Dearm Fields	181.25	25.38 ± 12.33	N.A.	N.A.
Ablation Studies	E_T+D	181.88	20.97 ± 13.59	38.61	N.A.
	w/o Stage 1	222.96	1.92 ± 2.22	79.41	N.A.
	w/o Stage 2	202.33	29.52 ± 14.86	41.71	N.A.
	w/o L_{bg_1}	149.45	29.45 ± 14.67	40.85	N.A.
	w/o L_{bg_2}	156.52	31.55 ± 8.87	38.31	N.A.
	w/o L_{bg}	178.34	30.96 ± 15.49	40.98	N.A.
Text2Image+SVR	GLIDE+DVR	212.41	8.85 ± 7.94	41.33	N.A.
	LAFITE+DVR	135.01	52.12 ± 11.05	37.55	11.70 ± 4.11
Ours	ISS	124.42 ± 5.11	60.0 ± 10.94	35.67 ± 1.09	21.70 ± 5.19

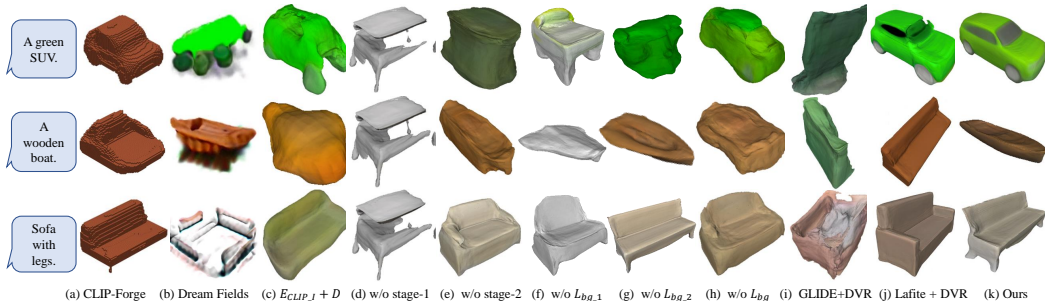


Figure 5: Qualitative comparisons with existing works and baselines.

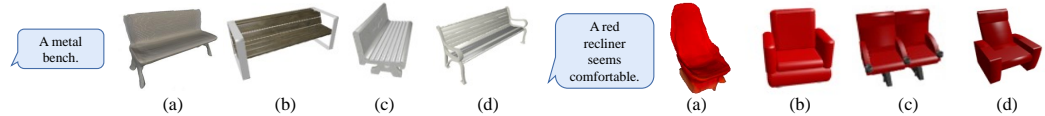


Figure 6: Our approach is able to generate novel shapes, not in the training set. (a) shows our results and (b,c,d) are the top-three shapes retrieved from the training set.



Figure 7: Our approach can generate diversified results from the same input text.

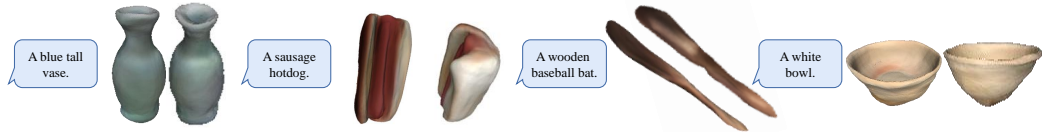


Figure 8: Results on CO3D dataset. We show two different views of each result.

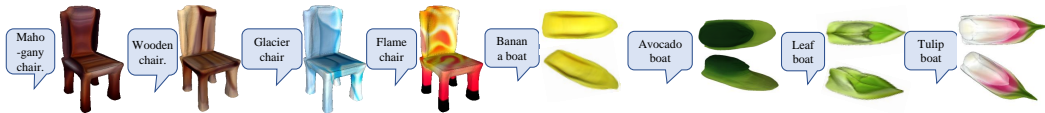


Figure 9: Text-guided stylization. Left: texture stylization. Right: shape-and-texture stylization.

4.4 MORE ANALYSIS ON GENERATIVE RESULTS OF ISS

Next, we present evaluations on the generative novelty and diversity, as well as the scalability of our two-stage feature-space alignment. Then, we show more text-guided stylization results and how our ISS approach generalizes to a wide range of categories and generates shapes with better fidelity.

Generation novelty. Our approach is able to generate novel shapes beyond simple retrieval from the training data. As shown in Figure 6, from the input text, we first generate our result in (a) and then take our generated shape to retrieve the top-three closest shapes in the associated training set

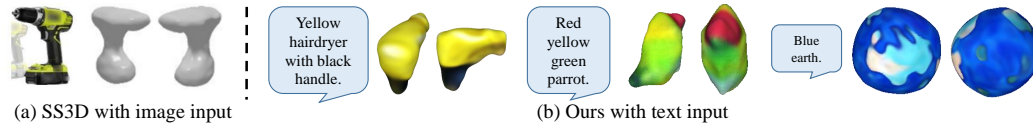


Figure 10: With single images for training (without camera poses), our approach can produce results for a broad range of categories, by adopting (Alwala et al., 2022). Two different views are rendered.

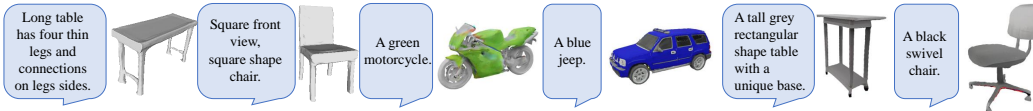


Figure 11: Results of ISS built upon the SVR model of IM-Net (left two) and GET3D (right four).

based on the cosine similarity between the CLIP features of the rendered images f_I and input text f_T as the retrieval metric. Our results with the two-stage feature-space alignment are not in the training sets, showing that our ISS approach can generate novel shapes beyond the training set, even without stylization. It is not surprising, as our approach shares the generative space with the pre-trained SVR model and can potentially generate all shapes that the pre-trained SVR model can produce.

Generation diversity. By perturbing the features and injecting randomness on initialization, ISS is able to generate diversified results from the same text input. As shown in Figure 7, ISS produces various cars and chairs from the same piece of text. Quantitative results are presented in the supplementary material Section 3.4 where our method achieves a high PS (Point Score).

Generation fidelity. To assess the capability of ISS in generating realistic real-world 3D shapes, we train the SVR model on the CO3D dataset (Reizenstein et al., 2021) which is a real-world dataset, and ISS leverages the learned feature space for text to shape generation without paired data. As shown in Figure 8, our model is able to generate real-world shapes. As far as know, this is first work that investigates text-guided shape generation and on real-world datasets can generate realistic 3D shapes.

Generation beyond the capability of SVR model. Our text-guided stylization module equips our model with the capability to generate 3D shapes beyond the SVR model. As shown in Figure 9 and Figure 2 (c), our model is able to create realistic and fantasy novel structures and textures that match text descriptions. Please refer to the supplementary material Section 4 for more details.

Generality and Scalability of ISS on other SVR models. Our model is generic and can work together with other SVR models. To evaluate the generality and scalability of our model, we employ SS3D (Alwala et al., 2022), IM-Net (Chen & Zhang, 2019), and GET3D (Gao et al., 2022) as SVR models to provide the feature space. It is worth noting that SS3D is capable of generating shapes of more categories and IM-Net, GET3D can produce high fidelity results. First, as shown in Figure 10, built upon SS3D, our approach can generate shapes of more real-world categories, *e.g.*, bird. Note that our model can generate shapes with comparable or even better qualities compared with initial SS3D model that takes an image as input. Second, when combined with IM-Net and GET3D, our model can fully exploit their generative capabilities and produces high-quality 3D shapes as shown in Figure 11. The above manifests that ISS is generic and compatible to advanced models for generating shapes of more categories and higher qualities.

5 CONCLUSION

In this paper, we present a novel approach for text-guided 3D shape generation by leveraging the image modality as a stepping stone. Leveraging the joint text-image embeddings from CLIP and 3D shape priors from a pre-trained SVR model, our approach eliminates the need for the paired text and shape data. Technically, we have the following contributions. First, we step-by-step reduce the semantic gap among the text, image and shape modalities through our two-stage feature-space alignment approach. Second, our text-guided stylization technique effectively enriches our generated shapes with novel structures and textures in various styles. Third, our approach is compatible with various single-view reconstruction approaches and can be further extended to generate a wide range of categories with only single images without camera poses in training. Experiments on ShapeNet,

CO3D, and multiple single-image categories manifest the superiority of our framework over the two state-of-the-art methods and various baselines. Limitations are discussed in the supplementary files.

Supplementary Material

In this supplementary material, we first introduce the background augmentation in text-guided shape stylization (Section 6). Next, we present the implementation details and evaluation metrics, and provide the details of human perceptual evaluation results (Section 7). Then, we introduce the setup and analysis of our ablation studies (Section 8). After that, we discuss text-guided stylization and provide more results (Section 9). Then we show additional generative results of our approach (Section 10). Further, we discuss two alternative training strategies (Section 11). Then, we show how feature is mapped in the latent space (Section 12) and also review some related literatures about SVR and differentiable rendering (Section 13). Afterwards we compare the number of parameters in our model and existing works (Section 14). We also discuss failure cases (Section 15) and limitations of this work (Section 16). Finally, we provide our text sets (Section 17) and summarize the notations in the paper (Section 18).

6 BACKGROUND AUGMENTATION IN TEXT-GUIDED SHAPE STYLIZATION

One important thing in text-guided shape stylization is that the generated texture should align with the given shape. However, it cannot be ensured with a simple white or black background during training since the generated textures can be affected by the background color. As shown in Figure 12 (a), the shape in white color may confuse with the white background; thus, the model would struggle to capture the boundary of objects, hence cannot generate textures that well-align with the table. In Figure 12 (c), the generated texture is severely affected by the black background color, causing low-quality stylization results.

To address the above issue, we propose a background augmentation strategy to improve the alignment between texture and shape. Specifically, the background color is replaced with random RGB values in each training iteration. By this means, the foreground shape may be more easily captured in training as shown in Figure 12 (b,d), improving the texture-shape consistency and the stylization quality.

Discussion on L_{bg} and background augmentation. In two-stage feature space alignment (Section 3.3 in the main paper), we introduce a background loss L_{bg} to encourage the color prediction on the background region to be white. A natural question is whether we can use background augmentation as a replacement, and our answer is no. As shown in Figure 13 (a), the background color can affect the cosine similarity of CLIP features between the image and input text; thus, using different background color in each iteration makes stage-2 alignment unstable and affects shape generation. As a result, the two-stage alignment can only benefit from L_{bg} , but not from the background augmentation, for producing a plausible shape. Besides, we empirically found that the two-stage feature space alignment with L_{bg} performs well, even if a white shape is being considered, see the bottom row in Figure 16 (i).

7 IMPLEMENTATION DETAILS, METRICS, AND HUMAN PERCEPTUAL EVALUATION DETAILS

Implementation details. Our framework is implemented using PyTorch (Paszke et al., 2019). We first train the stage-1 CLIP-image-to-shape mapping for 400 epochs with learning rate $1e^{-4}$, and then train the stage-2 text-to-shape module at test time for 20 iterations which takes only 85 seconds on average on a single GeForce RTX 3090 Ti. Optionally, we can further train text-guided stylization with the same learning rate. We empirically set hyperparameters $\lambda_M, \lambda_{bg}, t, m, \tau_1, \tau_2$ to be 0.5, 10, 0.5, 10, 0.2, 0.95, respectively, according to a small validation set.

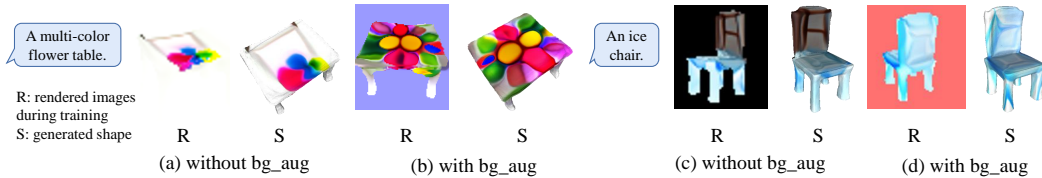


Figure 12: Effective of text-guided shape stylization with/without background augmentation.

Details on camera poses. In Stage 1, we follow Niemeyer et al. (2020) to set the camera poses to encourage the background to be white. Specifically, we randomly sample the distance of the camera and the viewpoint on the northern hemisphere.

In Stage 2, compared with Niemeyer et al. (2020), we sample the camera distance to be 1.5 times further compared with Niemeyer et al. (2020). It helps to encourage sampling more global views instead of only local ones, so that the CLIP image encoder can capture the whole shape and yield a better CLIP feature.

In Stage 3, we also sample the camera distance to be 1.5 times. Since this stage aims to generate textures instead of searching for a target shape like Stages 1 and 2, only sampling view points on the northern hemisphere of the view space cannot ensure good generation quality in the bottom regions. Thus, we further randomly sample viewpoints on the southern hemisphere for random 10% training iterations to encourage the stylized results to be consistent with the text in various viewpoints.

Decoder duplication Except for the output layer, we simply duplicate them to be D_o and D_c . For the output layer, it takes d -dimensional features as input and outputs one value for occupancy and three values for RGB. We then copy $d \times 1$ weights to D_o and copy $d \times 3$ weights to D_c . See Figure 15 for more details.

Metric: Shape generation quality. To measure the shape generation quality, we employ Fréchet Inception Distance (FID) (Heusel et al., 2017) between five rendered images of the generated shape with different camera poses and a set of ground-truth ShapeNet or CO3D images. We adopt the official model with Inception Net trained on ImageNet, which is widely used to evaluate generative quality and realism. We do not train a model on ShapeNet, since it is too small to train a better network for evaluating the FID than models trained on ImageNet. In addition, we randomly sample 2600 images in the ShapeNet dataset as ground truths for FID evaluation, instead of using images from ImageNet. It helps to measure the similarity between the generated shapes and ground truths of ShapeNet.

Besides adopting FID, we further utilize the metric Fréchet Point Distance (FPD) proposed in (Liu et al., 2022) to measure the shape generation quality without texture. We first convert the generated shapes to 3D point clouds without color (see Figure 14) and then evaluate FPD. Note that Dream Field (Jain et al., 2022) does not produce 3D shapes directly, so that we cannot evaluate this work in this regard.

To further assess the text-shape consistency, we conduct a human perceptual evaluation which is detailed as follows.

Human perceptual evaluation Setup. First, we prepare generated results for human evaluation. For each input text, we produce nine results from state-of-the-art methods, including CLIP-Forge (Sanghi et al., 2022) and Dream Fields (Jain et al., 2022), six baseline methods, and our full method; see Section 4.2 in the main paper and Section 8.1 in this supplementary material for details of each baseline. Second, we invite 10 volunteers (3 females and 7 males; aged from 19 to 58; all with normal vision) to evaluate the results. We show these results to the participants in random order without revealing how each result is produced. Then, they are asked to give a score from $\{1, 0.5, 0\}$ (1: perfect match, 0.5: partial match; and 0: don't match) on the degree of match between the generated shapes and input text. Then, for each method, we gather the evaluation scores from all participants and obtain the "Consistency Score" as s/n , where s is the total score and n is the number of samples.

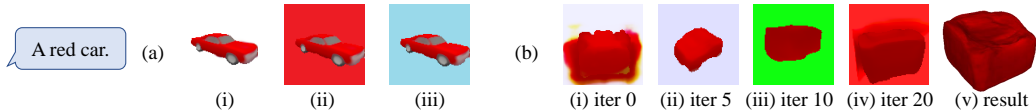


Figure 13: An investigation on background loss and background augmentation. (a) Background color affects the cosine similarity of the CLIP features between the image and the text “a red car”, *i.e.*, (i) 0.292 (ii) 0.303 and (iii) 0.285. (b) Effect of generating shapes with background augmentation, but without background loss L_{bg} . Comparing with Figure 4 (b) in the main paper, the two-stage feature space alignment works well with L_{bg} , but fails with the background augmentation.

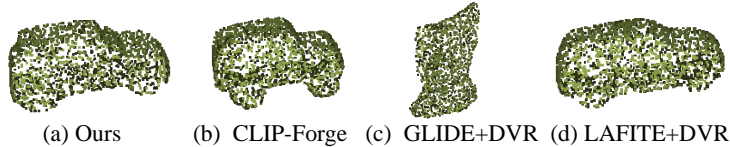


Figure 14: Visualization of point clouds of different methods for FPD evaluation.

Details of human perceptual evaluation results. We show Consistency Score and the preferences in the A/B/C test from each volunteer in Tables 2 and 3. As shown in Table 2, all ten volunteers consistently give the highest Consistency Score to our approach, and in the A/B/C test (see Table 3), all ten volunteers prefer results from our approach. The above further manifest the superiority of our model.

8 ABLATION STUDIES

8.1 BASELINE SETUPS

We create the following baselines in our ablation study. The first four baselines aim to assess the effectiveness of key modules in our approach, whereas the last two adopt state-of-the-art text-to-image generation approaches to first create images then adopt DVR (Niemeyer et al., 2020) to generate shapes for a fair comparison with our approach. Note that we do not adopt the most recent SVR model SS3D (Alwala et al., 2022) (which aims to work with in-the-wild images), due to its inferior generative quality and lack of texture generation.

- $E_1 + D$: As the first empirical study in Section 3.2 in the main paper, E_1 is adopted to extract the image feature f_1 and D is trained for 3D shape generation from f_1 without the two-stage feature-space alignment.
- w/o Stage 1: Stage-2 alignment is optimized from randomly initialized M , without stage 1.
- w/o Stage 2: Generate with M after stage 1, without the test-time optimization of stage 2.
- w/o L_{bg_1} : Remove L_{bg} in stage-1 alignment.
- w/o L_{bg_2} : Remove L_{bg} in stage-2 alignment.
- w/o L_{bg} : Remove L_{bg} in both stage-1 and stage-2 alignment.
- GLIDE+DVR: Use a recent zero-shot text-guided image generation approach GLIDE (Nichol et al., 2021) to generate image I from T , then use DVR (Niemeyer et al., 2020) to generate S from I .
- LAFITE+DVR: Train a recent text-guided image generation approach LAFITE (Zhou et al., 2022) with ShapeNet images, then generate image I from T . Further generate S from I with DVR (Niemeyer et al., 2020).

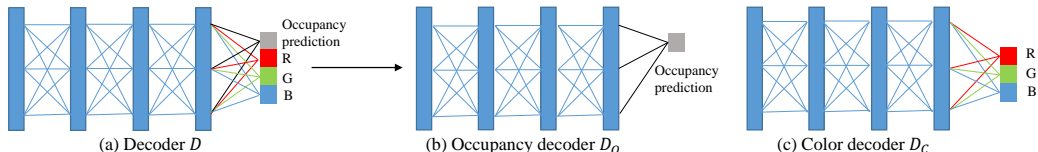


Figure 15: Visualization to duplicate the decoder D to D_o , D_c .

Table 2: Total scores s from the ten volunteers out of 52 generated shapes.

Method	1	2	3	4	5	6	7	8	9	10	mean \pm std	Consistency Score (%) \uparrow
CLIP-Forge	21	35	34	16.5	18.5	29	21.5	4	21	17	21.75 \pm 9.16	41.83 \pm 17.62
Dearm Fields	13	17.5	7	19	6.5	22	22	9	10	6	13.2 \pm 6.41	25.38 \pm 12.33
E_1+D	14	9.5	5	18	4.5	25	15.5	4.05	4.5	9	10.91 \pm 7.06	20.97 \pm 13.59
w/o stage-1	1.5	1	0	1.5	0	3.5	2	0	0	0.5	1.00 \pm 1.15	1.92 \pm 2.22
w/o stage-2	20	14.5	8.5	23.5	7.5	27	19	8.5	4.5	20.5	15.35 \pm 7.73	29.52 \pm 14.86
w/o L_{bg}	17.5	15.5	8.5	21	8	27	26.5	9.5	5	22.5	16.1 \pm 8.06	30.96 \pm 15.49
GLIDE+DVR	5	3.5	1.5	10	2	13	6.5	0.5	1	3	4.60 \pm 4.13	8.85 \pm 7.94
LAFITE+DVR	23	33.5	31	23	27	31.5	27.5	14.5	32.5	27.5	27.10 \pm 5.75	52.12 \pm 11.05
ISS (ours)	32	37	35.5	29.5	29	37	29	17.5	32.5	33	31.20 \pm 5.69	60.00 \pm 10.94

Table 3: A/B/C Test results of the ten volunteers. The numbers in the table indicate the number of shapes from the corresponding method he/she likes most out of the three candidates. Volunteers can optionally select “pass” instead of “A/B/C” if he cannot decide which one is the best.

Category	Method	1	2	3	4	5	6	7	8	9	10	mean \pm std \uparrow
Existing works	CLIP-Forge	9	17	12	13	6	9	3	6	6	8	8.9 \pm 4.12
SOTA Text2Image+SVR	LAFITE+DVR	9	16	9	12	7	13	9	20	8	14	11.7 \pm 4.11
Ours	ISS	27	19	21	20	17	25	19	26	13	30	21.7 \pm 5.19

8.2 QUANTITATIVE AND QUALITATIVE COMPARISONS

In this section, we analyze the results of the above baselines one by one.

- $E_1 + D$: column (c) shows that the results generated from CLIP space Ω_1 have inferior fidelity in terms of the texture (top row in Figure 16) and shape structure (bottom two rows in Figure 16) due to the limited capability of E_1 to capture details of the image.
- w/o Stage 1: column (d) of Figure 16 indicates that without stage-1 alignment, the generated shape are almost the same whatever text T is adopted as input, since M tends to map text feature f_T to almost the same feature even though stage-2 alignment is enabled. It shows that a good initialization provided by stage-1 alignment is necessary for the test-time optimization of stage 2.
- w/o Stage 2: as shown in column (e) of Figure 16, without Stage 2, may not align well with f_S due to the semantic gap between f_I and f_T . Now, we use Figure 17 (a) to illustrate their associated results: the model in “w/o stage 2” can generate reasonable shapes from a single image (see “SVR” in Figure 17 (a)) but fails with text as input (see “stage 1” in Figure 17 (a)); further with the stage-2 optimization, a plausible phone can be generated (see “stage 2 (ours)” in Figure 17 (a)). w/o L_{bg_1} , w/o L_{bg_2} , w/o L_{bg} : stage-2 alignment cannot work properly without L_{bg} in either stage-1 or stage-2 alignment or both (see column (f, g, h) of Figure 16) due to the lack of foreground awareness. Even though stage-1 alignment has encouraged the background to be white, we still need this loss in stage 2 to get satisfying results.
- GLIDE+DVR: the images created by GLIDE (Nichol et al., 2021) have a large domain gap from the training data of DVR (see Figure 17 (b)), severely limiting the performance of GLIDE+DVR (see Figure 16 (i)).
- LAFITE+DVR: as shown in Figure 16 (j), some generative results of LAFITE+DVR can be coarse (first row of the main paper and the last row of Figure 16 in this supplementary material) due to the error accumulation of the isolated two steps, *i.e.*, LAFITE (see Figure 17 (b) “image from LAFITE”) and DVR, and some do not match the input text due to the semantic gap between f_I and f_T (two bottom rows of Figure 5 in the main paper and the last row of Figure 16 in this supplementary material). Despite the above, subsequently generating images then shapes is still a strong baseline that is a valuable research direction in the future.
- ours (ISS): column (k) of Figure 5 in the main paper and Figure 16 in this supplementary material show that our approach can generate shapes and textures with good text-shape consistency (see “small wings” in the top row, “water craft” in the middle row of Figure 16) and fidelity, beyond all the above baselines and the existing works CLIP-Forge (Sanghi et al., 2022) and Dream Field (Jain et al., 2022).

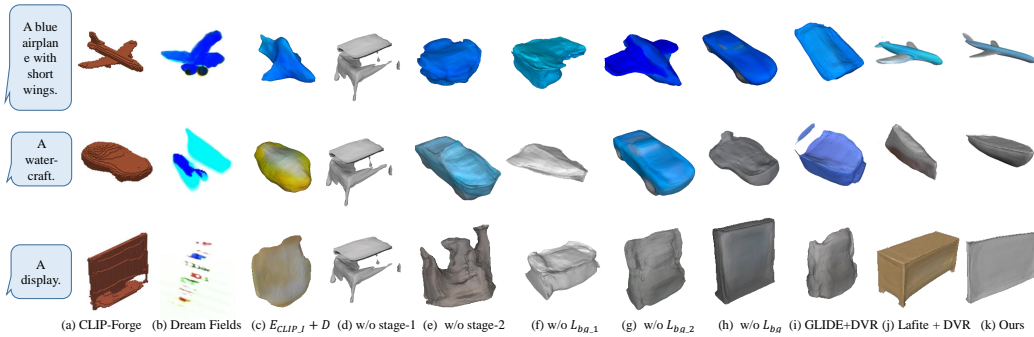


Figure 16: Additional qualitative results compared with existing works and baselines.

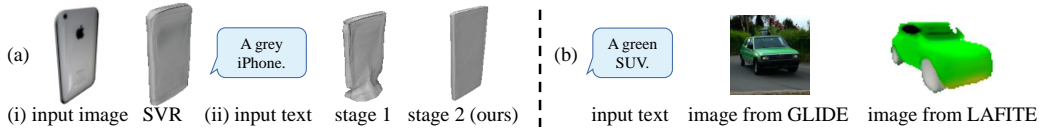


Figure 17: A further investigation on baselines “w/o stage 2”, “GLIDE+DVR”, and “LAFITE+DVR”. (a) “w/o stage 2” produces a plausible shape (“SVR”) from image but a low-quality shape (“stage 1”) from text; further fine-tuning using stage-2 alignment enables us to produce a more plausible shape from text (“stage 2 (ours)”). (b) GLIDE / LAFITE generate out-of-domain and inferior-quality images, limiting the performance of subsequent 3D generation.

8.3 A/B/C TEST

To further compare our approach with the strongest baselines CLIP-Forge (Sanghi et al., 2022) and “LAFITE+DVR”, we perform an A/B/C test with 10 volunteers to compare these two baselines with ours. Specifically, the results from the three approaches (per input text) in random order for all the 52 texts. Then, they were instructed to choose a most preferred one. The results in Table 1 “A/B/C Test” in the main paper show that our results are more preferred than others, outperforming (Sanghi et al., 2022) by 143.8% $((21.70 - 8.90)/8.90)$ and “LAFITE+DVR” by 85.5% $((21.70 - 11.70)/11.70)$.

8.4 DIVERSIFIED GENERATION

In addition, we evaluate the diversified generation results discussed in Section 3.3 in the main paper. Specifically, we generate additional two samples per input text, and then adopt FID (Heusel et al., 2017), FPD (Liu et al., 2022) (the lower, the better) for the fidelity evaluation and Point Score (PS) (Liu et al., 2022) (the higher, the better) for the diversity evaluation. The results are: **FID: 113.42**, **FPD: 33.66**, **PS: 3.58**, which is even better than our one-text-one-shape generative results (FID: 124.42 ± 5.11 , FPD: 35.67 ± 1.0 , PS: 3.18 ± 0.11), manifesting the superior performance of diversified generation capability of ISS..

9 DISCUSSIONS ON TEXT-GUIDED SHAPE STYLIZATION

Additional stylization results. As shown in Figure 18 (a), our text-guided shape stylization is able to generate vivid landscape and flower textures on the sofa shape. Note that the sofa is generated from the text “A sofa with black backrest” (see Figure 20 top right) with totally different initial color from the stylization results. Further, in Figure 18 (b), we show four additional texture stylization results in addition to the Figure 9 in the main paper. In addition, as shown in Figure 18 (c), our shape-and-texture stylization is able to generate novel shapes and textures beyond the dataset, and create imaginary shapes with diversified structures. Note that our results achieve a good balance on the stylization and the functionality. For example, our result of “avocado chair” possesses both the style of “avocado” and the functionality of “chair”.

As shown in Figure 19, shape-and-texture stylization consistently produces the cars that is consistent with the input text “a blue car”, with proper variation in terms of the color and shape. In addition, the degree of the shape variations can be controlled by the loss weight λ_P of the 3D prior loss L_P .

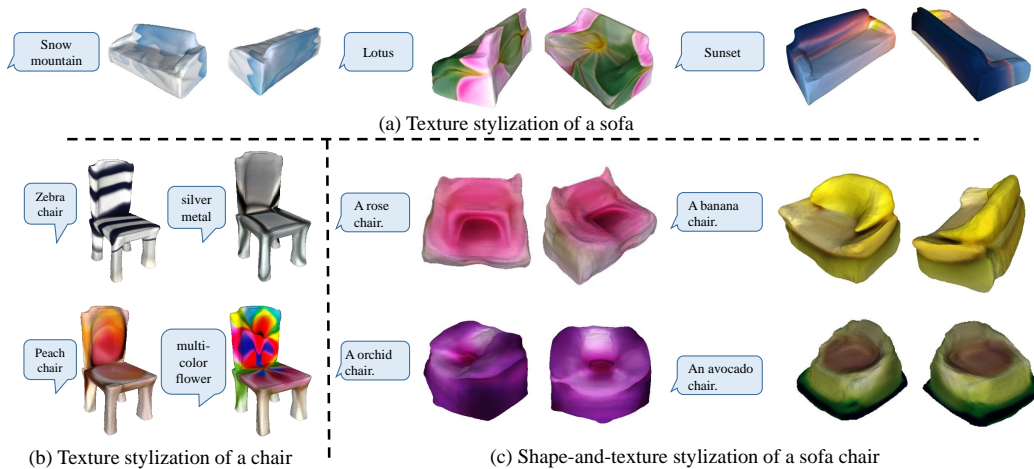


Figure 18: Additional stylization results.

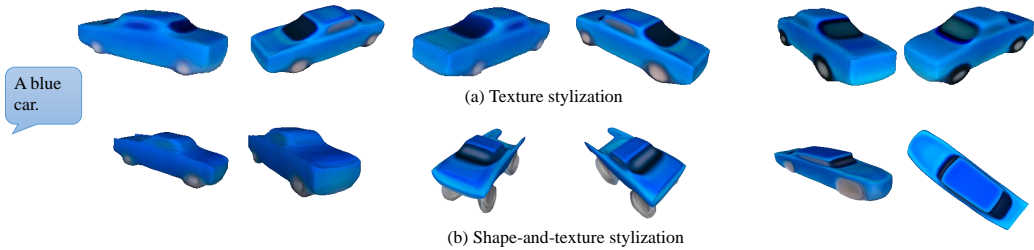


Figure 19: Results of shape-and-texture stylization with the same text “A blue car” and different 3D prior loss L_P .

Why does shape-and-texture stylization need a initial shape? Shape-and-texture stylization is initialized by the two-stage feature-space alignment result, since it provides the 3D prior.

Relationship of texture stylization and shape-and-texture stylization. Texture stylization and shape-and-texture stylization have their own merits. Texture stylization keeps the shape unchanged and is able to guarantee the functionality of the shape. In addition, it can take some abstract text descriptions as input like “sunset” in Figure 18 (a). Shape-and-texture stylization is able to generate novel and imaginary structures beyond the training dataset. However, there is a tradeoff between the stylization and the functionality.

10 ADDITIONAL RESULTS

ShapeNet. As shown in Figure 20, our approach can generate view-consistent 3D shapes on ShapeNet (Chang et al., 2015) that well match the input texts.

CO3D. Further, we show more text-guided shape generation results on the CO3D (Reizenstein et al., 2021) dataset in Figure 21. These results again manifest the capability of our approach on real-world 3D shape generation, beyond the existing works (Chen et al., 2018; Sanghi et al., 2022; Liu et al., 2022) that focus only on the synthetic shape generation on ShapeNet (Chang et al., 2015).

Working with GET3D When working with GET3D (Gao et al., 2022), our approach can generate 3D shapes of good fidelity from texts, as shown in Figure 22 in this supplementary file.

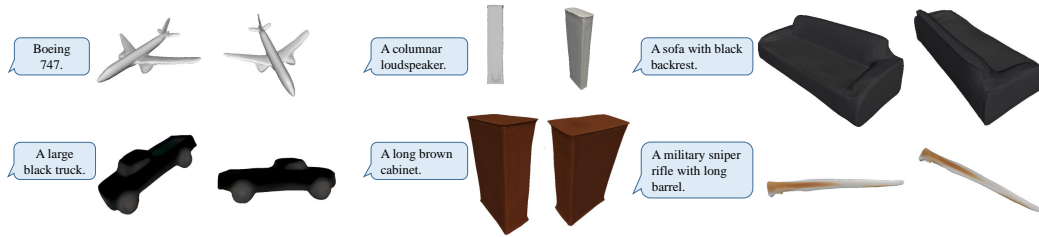


Figure 20: Additional generative results on the ShapeNet (Chang et al., 2015) dataset.

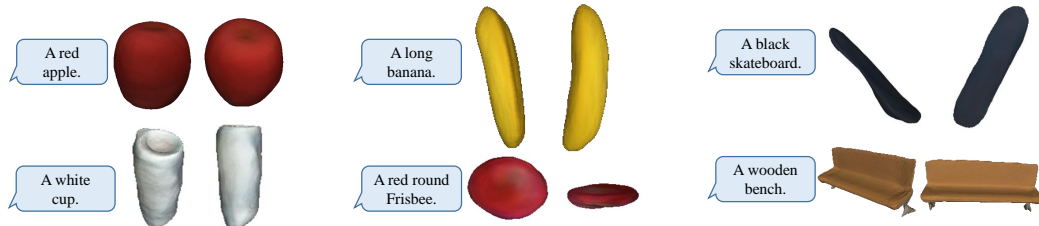


Figure 21: Additional generative results on the CO3D (Reizenstein et al., 2021) dataset.

Single-image categories. In Figure 23, we present more text-guided generations for more categories using single images in training without camera pose, built upon Alwala et al. (2022). The results further demonstrate the compatibility of our approach to various SVR approaches, particularly generating plausible 3D shapes from text with single images in training.

More generative results. Further, we present more generative results of our approach in Figure 24. Using ISS, we are able to effectively generate a wide variety of 3D shapes from texts.

11 DISCUSSIONS ON TWO ALTERNATIVE TRAINING STRATEGIES

Fine-tune decoder. In this section, we discuss an alternative training strategy to optimize the decoder directly with the CLIP consistency loss, instead of using two-stage feature space alignment.

First, we provide the results of the above training strategy. It produces unsatisfactory 3D shapes such as the one shown in Figure 25 (c) with more than 20 minutes of training. Besides, Dream Field (Jain et al., 2022) also utilizes the same idea to optimize the decoder directly; yet, the generated shape (see Figure 25 (d)) is also far from satisfactory even though Dream Fields is trained only to produce multi-view images with an NeRF-like architecture, unlike ours that is capable for 3D shape generation.

Then we try to analyze why the above strategy fails to produce desired shapes. Leveraging the pre-trained decoder that has already incorporated the 3D shape prior, our approach is able to search for the desired shape in the shape feature space Ω_S efficiently. On the contrary, fine-tuning the decoder in stage 2 without the explicit 2D/3D supervision will destroy the pre-trained shape feature space Ω_S , which is used to introduce 3D priors. Specifically, in stage 2 (“alignment stage”), the model is trained at test time with the user-provided text without any explicit 2D/3D supervision, so it is hard for the model to gain the knowledge about what the desired 3D shape should be like. In

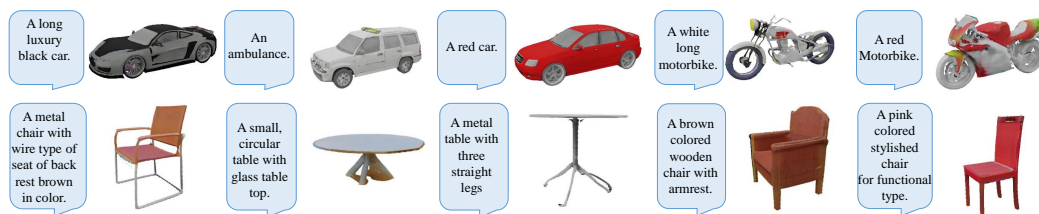


Figure 22: Additional generative results built upon GET3D (Gao et al., 2022).

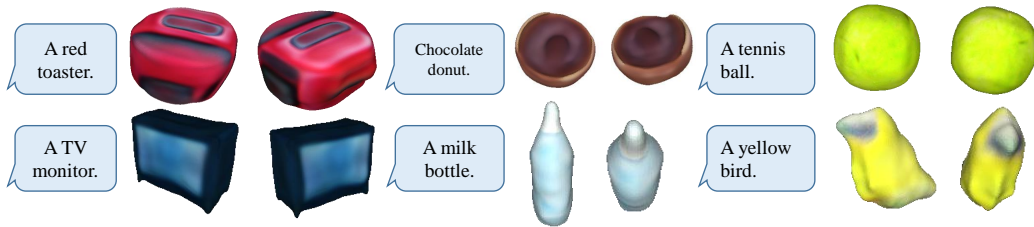


Figure 23: Additional generative results built upon SS3D (Alwala et al., 2022) using single images in training without camera pose.

other words, it is extremely challenging for the model to learn the 3D shape prior with only CLIP consistency supervision from text.

Further, we analyze why the decoder can be fine-tuned in shape-and-texture stylization. First, note that 3D shape generation is a very different task from shape-and-texture stylization, since shape-and-texture stylization is initialized by the two-stage feature-space alignment result, which has already learned the 3D prior. Therefore, we can fine-tune the decoder in shape-and-texture stylization.

Update the feature in the shape space. In this section, we discuss another alternative training strategy to optimize the feature in shape space Ω_S , instead of optimizing the mapper M with stage-2 feature space alignment.

However, the shape feature has only 256 dimensions, which is far smaller than the number of weights in the mapping network. Hence, directly optimizing the shape feature in Ω_S is not capable for generating the desired 3D shape as shown in Figure 26, and the stage-2 feature space alignment is necessary in our approach.

12 ANALYSIS ON FEATURE SPACE MAPPING

To provide more insights on explaining how the latent space is mapped, we measure the distance of features at different stages on all the samples in our test set on ShapeNet in Table 4. The notations follow Figure 3 (c) of the main paper, M means the mapper, and d means cosine distance. Our ultimate goal is to obtain a text mapper M' (Figure 2 in the main paper) to map the text feature space f_T to shape feature space f_S using image with features f_I as a stepping stone to gradually narrow their distances using two stage mapping. Note that the image f_I and text features f_T are obtained using pre-trained CLIP models.

In the stage-1 alignment process, we train a mapper M to map image features f_I to a space $M(f_I)$ close to the shape space f_S using image data and the regression loss L_M . Note that the text feature f_T and image feature f_I are all from the CLIP model in a shared embedding space. It's natural that the trained mapper can be used to map the text feature f_T to $M(f_T)$, making text features closer to the shape space. However, when measuring the distance among $M(f_I)$, $M(f_T)$, we find the average distance among all samples is $d(M(f_I), M(f_T)) = 0.58 \pm 0.23$, the average distance between $M(f_I)$ and f_S is 0.21 ± 0.10 , and the average distance between shape and text is $d(M(f_T), f_S) = 0.45 \pm 0.20$. This implies that there is a gap between CLIP image and text feature after the first step mapper and further motivates our stage-2 alignment. Note that there is no GT shape for our task on 3D generation, so we manually select a shape in the ShapeNet dataset that matches the input text as the GT.

In the stage-2 alignment, M is further updated and the final delivered mapper is called M' which is to further narrow down the gap between mapped text features and shape features. The average distance between the mapped text feature $M'(f_T)$ and shape feature space f_S : $d(M'(f_T), f_S) = 0.17 \pm 0.08$ which is much smaller than the corresponding distance after stage-1 alignment. It shows that stage 2 alignment can significantly reduce the difference between the mapped text and the GT shape feature from 0.45 to 0.17 on average.



Figure 24: Generative results of ISS. Using our new approach, we are able to effectively produce 3D shapes for a wide variety of categories from texts.

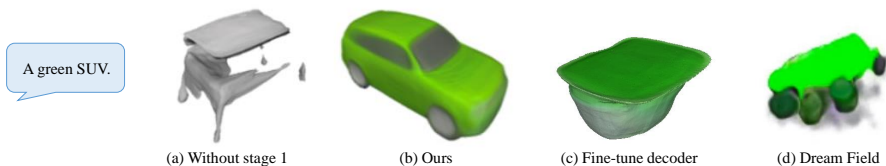


Figure 25: Results of optimizing the decoder, instead of the two-stage feature-space alignment.

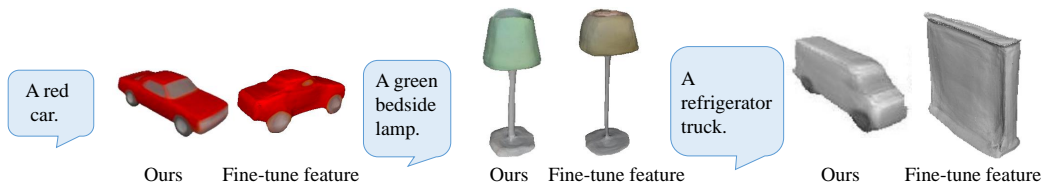


Figure 26: Results of optimizing the feature in shape space, instead of the stage-2 feature-space alignment.

Table 4: Distance changes in the feature space mapping of all the 52 samples in the test set. d means cosine distance. Almost all distances are consistently reduced after our stage-2 alignment.

Text	$d(M(f_I), M(f_R))$	$d(M(f_I), f_S)$	$d(M(f_R), f_S)$	$d(M'(f_R), f_S)$	$d(M(f_R), M'(f_R))$
a glass single leg circular table	0.63	0.31	0.58	0.14	0.34
a wooden double layers table	0.72	0.10	0.64	0.14	0.65
a square metal table	0.76	0.32	0.44	0.21	0.30
a round shaped single legged wooden table	0.47	0.24	0.21	0.21	0.30
this is a bar stool with metal arches as a design feature	0.43	0.33	0.35	0.18	0.17
a children chair with little legs	0.79	0.20	0.43	0.12	0.35
a swivel chair with wheels	0.61	0.30	0.38	0.22	0.11
a red recliner seems comfortable	0.33	0.20	0.23	0.24	0.05
a red car	1.02	0.19	0.78	0.10	0.69
a green SUV	0.49	0.12	0.24	0.19	0.25
a large black truck	0.74	0.19	0.50	0.15	0.53
a long luxury black car	0.67	0.22	0.54	0.09	0.54
army fighter jet	0.43	0.54	0.43	0.25	0.28
a black airplane with long white wings	0.62	0.12	0.32	0.16	0.10
a blue airplane with short wings	0.51	0.14	0.55	0.33	0.40
boeing 747	0.35	0.13	0.23	0.06	0.20
a big ship for transportation	0.95	0.17	0.72	0.35	0.21
a boat with sail	0.39	0.19	0.46	0.12	0.45
a watercraft	0.12	0.14	0.27	0.22	0.06
a wooden boat	0.76	0.29	0.52	0.12	0.49
a blue sofa	0.46	0.20	0.34	0.12	0.27
sofa with legs	0.67	0.13	0.55	0.10	0.35
a sofa with black backrest	0.59	0.14	0.33	0.08	0.16
a small sofa	0.49	0.20	0.33	0.10	0.28
a long brown bench	0.57	0.29	0.34	0.18	0.27
a marble bench	0.61	0.16	0.46	0.12	0.29
a metal bench	0.18	0.29	0.20	0.20	0.09
concrete bench	0.48	0.07	0.46	0.11	0.36
a military sniper rifle with long barrel	0.47	0.14	0.29	0.07	0.21
a rifle with magazines	0.71	0.48	0.51	0.17	0.43
a short rifle	0.75	0.15	0.81	0.35	0.52
rifle shotgun	0.38	0.13	0.25	0.10	0.09
a computer monitor	0.28	0.07	0.22	0.07	0.20
a display	0.22	0.18	0.15	0.13	0.02
a monitor with square base	0.56	0.17	0.75	0.33	0.34
a TV monitor	0.70	0.16	0.41	0.11	0.27
a cabinet with cylindrical legs	0.53	0.24	0.27	0.18	0.11
a cupboard	0.54	0.37	0.42	0.19	0.45
a long brown cabinet	0.57	0.29	0.34	0.18	0.27
a wardrobe	0.41	0.13	0.32	0.16	0.26
a desk lamp	0.92	0.35	0.51	0.16	0.45
bedside lamp	0.71	0.48	0.55	0.17	0.43
lamp supported by a long pillar	0.19	0.12	0.18	0.05	0.14
mushroom-like lamp	1.20	0.17	1.06	0.32	0.46
a mobile phone	0.75	0.09	0.85	0.28	0.55
a small cell phone	0.49	0.20	0.33	0.10	0.28
a mobile phone with black screen	0.94	0.39	0.61	0.14	0.68
an iphone	0.75	0.25	0.54	0.22	0.57
a columnar loudspeaker	0.66	0.25	0.54	0.15	0.40
a loudspeaker with metal surface	0.34	0.17	0.44	0.16	0.30
a wooden loudspeaker	0.72	0.10	0.64	0.14	0.65
a cylindrical loudspeaker	1.06	0.19	0.82	0.31	0.27
mean \pm std	0.58 \pm 0.234	0.21 \pm 0.10	0.45 \pm 0.20	0.17 \pm 0.08	0.32 \pm 0.17

Table 5: Number of parameters and performance of existing works and our method.

Method	Number of parameters (M)	FID	FPD	Consistency Score
CLIP-Forge (Sanghi et al., 2022)	Normalized flow network: 18.37	162.87	37.43	41.83±17.62
Dream Fields (Jain et al., 2022)	0.61	181.25	N.A.	25.38±12.33
Ours	Mapper: 2.43	124.42±5.11	35.67±1.09	60.0±10.94
Ours with a lightweight mapper	Mapper: 0.46	129.01	34.26	67.21±10.64

13 RELATED WORKS ON SINGLE-VIEW RECONSTRUCTION AND DIFFERENTIABLE RENDERING

Single-view reconstruction (SVR) This task aims to reconstruct the 3D shape from a single-view image of it. Recently, many approaches have been proposed for meshes (Agarwal & Gopi, 2020), voxels (Zubić & Liò, 2021), and 3D shapes (Niemeyer et al., 2020). Recently, to extend SVR to in-the-wild categories, Alwala et al. (2022) proposed a new approach called SS3D to learn 3D shape reconstruction using single-view images for the reconstruction of hundreds of categories.

As 3D-to-2D projections, single-view 2D images are more closely related to shapes than texts, since they reveal many attributes of 3D shapes, e.g., structure, details, appearance, etc. The strong correlation between 2D images and 3D shapes motivates us to reduce the challenging text-to-shape generation task to text-to-image and then SVR, by connecting the CLIP features from text with the shape features in SVR using images as an intermediate step to gradually bridge the gap between text and shape. Specifically, we extend the pre-trained SVR model to be compatible with text input, transforming the challenging text-to-shape task into SVR. Our framework can work with different SVR approaches to extend them for 3D shape generation from texts. So, our approach is orthogonal to the SVR approaches.

Differentiable Rendering 3D rendering is an important topic in computer vision and graphics. It takes a 3D scene as input and predicts the 2D view of it given a camera pose. Beyond 3D rendering, differentiable rendering further aims to derive the differentiations of the rendering function. With differentiable rendering, a renderer can be integrated into an optimization framework, thus a 3D shape can be reconstructed from multi-view 2D images. Neural Volume Rendering (Mildenhall et al., 2020) and its following works (Jain et al., 2021; Barron et al., 2021) aim to synthesize novel view images of a 3D scene. Besides, recent works (Niemeyer et al., 2020; Munkberg et al., 2022; Gao et al., 2022) leverage differentiable rendering for 3D shape generation using 2D images. In this work, we derive 2D images of the generated 3D shape using differentiable rendering and use a pre-trained large-scale image-language model CLIP to encourage the 2D images to be consistent with the input text. Thanks to differentiable rendering, we can update the generated 3D shape indirectly using the rendered images.

14 ANALYSIS ON THE NUMBER OF PARAMETERS

Our model incorporates only a small amount of learnable parameters for shape generation in M . Note that the parameters of the SVR model are not tuned for the specific text-to-shape generation task. Therefore, they are not counted in the total number of parameters.

We provide the comparison of learnable model parameters responsible for shape generation and compare it with existing methods in Table 5.

The number of learnable parameters of CLIP-forge (Sanghi et al., 2022) is 8 times larger than ours. Note that we do not include the parameters of the CLIP-Forge auto-encoder for a fair comparison. With much fewer parameters, our model outperforms CLIP-Forge in all evaluated metrics (see Table 5). This demonstrates that our performance gain is not purely from the learnable parameters.

To better compare with Dream Fields (Jain et al., 2022) (0.61 M parameters), we design a lightweight mapper to match the total number of parameters. Specifically, the mapper is composed of three fully connected layers with 512, 256, and 256 output dimensions, yielding a total of 0.46M parameters which is smaller than Dream Field. With this new mapper, we still outperform Dream Fields in terms

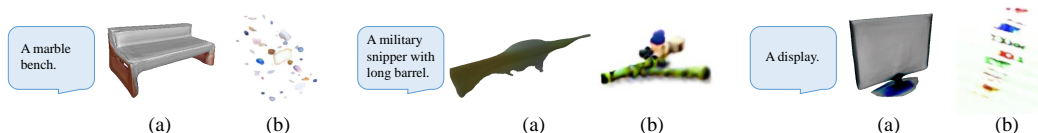


Figure 27: (a) Our generative result with lightweight mapper vs. (b) Dream Fields (Jain et al., 2022).

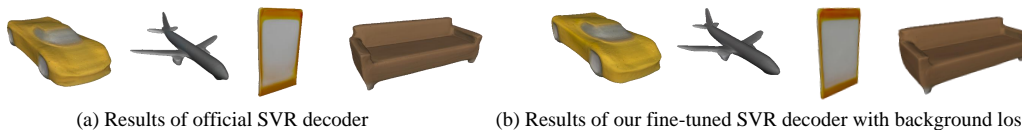


Figure 28: The generative results of the original SVR model and after our stage-1 feature space alignment using the same feature f_s .

of metrics. Please see Figure 27 for quantitative comparison. This further demonstrates our major performance gain is not from the learnable parameters.

From the results in Table 27, we can consistently observe that our model can achieve much better performance with much fewer parameters, manifesting the efficiency of our proposed image as a stepping-stone pipeline that allows us to leverage the 3D priors in pre-trained SVR models to enable text to 3D shape synthesis without requiring paired text and 3D data.

Note that we exclude the number of parameters of the decoder D in our comparison because the only effect of fine-tuning D is to make the background white and does not contribute to the generative capability of our model. As shown in Figure 2 of the main paper, mapper M and decoder D are trained with their own losses **separately** at the same time by stopping the gradients from L_D and L_{bg} to propagate to M .

Also, to show that fine-tuning D does not improve its generative capability, we feed the same input feature f_s to D before and after fine-tuning, they generate almost the exact same 3D shape as the original SVR model, as shown in Figure 28 in the supplementary material. And in stage 2, D is not optimized. Admittedly, our generative capability benefits from the SVR model including D . However, D is not optimized for our text-to-shape generation task. Therefore, we exclude the number of parameters of decoder D for fair comparison.

15 FAILURE CASES

Here are some examples of failure cases of our approach.

The complex and unusual shapes, e.g., “an oval table with 3 legs.” First, our model fails to generate the shape from the text “an oval table with 3 legs.”. Our approach leverages the CLIP consistency loss in the rendered 2D image; however, in the rendered image shown in Figure 29 (a), only three legs can be seen and the remaining one is occluded, which confuses the model training.

The given text is very long, e.g., “it is grey in color , circular in shape with four legs and back support, material used is wood and overall appearance looks like unique design armless chair.” Our model fails to generate the shape from the above long description as shown in Figure 29 (b). Some attributes are missing including “armless”, “four legs”. This is partially due to the limited representative capability of a single CLIP feature for such a long sentence. We may incorporate an additional local feature like Liu et al. (2022) to handle the long text in the future.

The shapes with multiple fine-grained descriptions, e.g., “A chair with a red back and a green cushion.” As shown in Figure 29 (c), our model fails to generate the shape “A chair with a red back and a green cushion.”. As studied in some recent works (Yao et al., 2022; Li et al., 2022), CLIP mainly address on the global image feature, but has inferior capability to capture fine-grained features. Therefore, our approach may fail to generate shapes where multiple fine-grained descriptions are

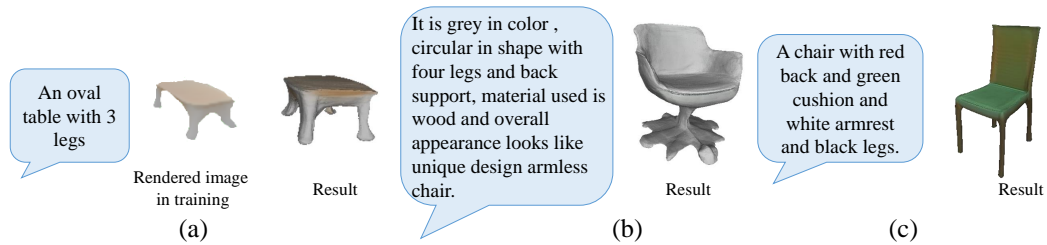


Figure 29: Failure cases of our approach.

given. In the future, we may try more recent pre-trained text-and-image embedding models to enhance the model’s capability to handle the fine-grained descriptions.

16 LIMITATIONS

This work still has some limitations. First, our performance is limited by the SVR model that our approach is built upon, *e.g.*, some results in Figure 10 of the main paper and Figure 23 in this supplementary material are still not very satisfactory, because SS3D (Alwala et al., 2022) itself is struggling to create shapes with fine details.

Second, we cannot generate the categories outside the image dataset due to the lack of 3D prior of the unseen category. That is why our model needs images as the stepping stone to learn what the particular category is like. However, we want to highlight the following. First, built upon SS3D (Alwala et al., 2022), our approach can generate a wide range of categories with single-view images in the wild as training data. Second, with our shape-and-texture stylization, our approach can generate imaginary and uncommon shapes outside the image dataset (in the same category). Third, it is extremely challenging to generate arbitrary category shapes from text. As far as we know, there is only one existing work, Dream Field (Jain et al., 2022), that can generate more categories than ours. However, Dream Fields only generate multi-view images instead of directly generate 3D shapes, and it cannot generate reasonable shapes in many cases as shown in Figure 5 in our main paper and Figure 8 in this supplementary material.

17 TEXT SET IN THE EXPERIMENTS

Recent works (Chen et al., 2018; Sanghi et al., 2022; Jain et al., 2022) proposed their own text sets. However, their datasets have some limitations and are not suitable to evaluate our approach. The dataset of Text2Shape (Chen et al., 2018) contains text descriptions in only two categories, *i.e.*, Table and Chair; CLIP-Forge (Sanghi et al., 2022) lacks of descriptions on the color and texture; while Dream Fields (Jain et al., 2022) utilizes text descriptions containing complex scenes and actions. To fairly evaluate our approach, we propose two text datasets on the ShapeNet (Chang et al., 2015) and CO3D (Reizenstein et al., 2021) categories, respectively, shown in Tables 7 and 8.

18 LIST OF NOTATIONS

In this section, we summarize symbols and notations used in the paper to facilitate readers to follow up. Please refer to Table 6 for more details.

REFERENCES

Nitin Agarwal and M Gopi. Gamesh: Guided and augmented meshing for deep point networks. In *3DV*, 2020.

Table 6: Summary of symbols used in paper.

Notation	Description	Notation	Description
E_S	encoder of SVR model	E_I	CLIP image encoder
E_T	CLIP text encoder	D	Decoder of SVR model
M	Mapper	M'	Mapper after stage-2 alignment
D_o	occupancy decoder	D_c	color decoder
R	rendered images	f_I	CLIP image feature
f_T	CLIP text feature	f_S	shape feature in SVR model
o	camera center	p	query point
d	cosine distance	L_M	regression loss in stage 1
L_D	original loss in SVR model	L_{bg}	background loss
$L_{bg,1}$	background loss in stage 1	$L_{bg,2}$	background loss in stage 2
L_C	CLIP consistency loss	L_P	3D prior loss
Ω_T	CLIP text feature space	Ω_S	shape feature space from the SVR model
Ω_I	CLIP image feature space		

Table 7: Texts on ShapeNet (Chang et al., 2015). They are utilized to measure FID (Table 1 of the main paper), and employed in Human Perceptual Evaluation (Table 2) and A/B/C Test (Table 3).

a glass single leg circular table	a wooden double layers table
a square metal table	a round shaped single legged wooden table
this is a bar stool with metal arches as a design feature	a children chair with little legs
a swivel chair with wheels	a red recliner seems comfortable
a red car	a green SUV
a large black truck	a long luxury black car
army fighter jet	a black airplane with long white wings
a blue airplane with short wings	boeing 747
a big ship for transportation	a boat with sail
a watercraft	a wooden boat
a blue sofa	sofa with legs
a sofa with black backrest	a small sofa
a long brown bench	a marble bench
a metal bench	concrete bench
a military sniper rifle with long barrel	a rifle with magazines
a short rifle	rifle shotgun
a computer monitor	a display
a monitor with square base	a TV monitor
a cabinet with cylindrical legs	a cupboard
a long brown cabinet	a wardrobe
a desk lamp	bedside lamp
lamp supported by a long pillar	mushroom-like lamp
a mobile phone	a small cell phone
a mobile phone with black screen	an iphone
a columnar loudspeaker	a loudspeaker with metal surface
a wooden loudspeaker	a cylindrical loudspeaker

Table 8: Texts on CO3D (Reizenstein et al., 2021).

A big apple	A red apple	A green bottle	A tall cylindrical bottle
A white cup	A wooden cup	A large black microwave	A white cuboid microwave
A black skateboard	A green long skateboard	A cute toytruck	A large toy truck
A blue backpack	A red big backpack	A white bowl	A big wooden bowl
A red round frisbee	A blue large frisbee	A big blue motorcycle	A black large wheels motorcycle
A circular stop sign	A triangle stop sign	TV screen	A grey big tv screen
A basketball	A tennis ball	A large broccoli	A green broccoli
A hairdryer	A yellow hairdryer	A black mouse	A white mouse
A cuboid big suitcase	A large size tall suitcase	A round umbrella	A big black umbrella
A big banana	A long banana	A cream round cake	A chocolate mooncake
A blue handbag	A red big handbag	An orange	A large round orange
A teddybear	A cute teddybear	A blue fat vase	A blue tall vase
A black baseball bat	A long wooden baseball bat	A blue car	A red car
An egg hotdog	A sausage hotdog	A black parkingmeter	A white tall parkingmeter
A black toaster	A round toaster	Tall wineglass	Single leg big wineglass
A brown baseball glove	A black big baseball glove	A big carrot	A long carrot
A red hydrant	A yellow hydrant	A large round pizza	A tomato meat pizza
A white toilet	A fat white toilet	A stone bench	A wooden long bench
A gray iphone	A black phone	A long black keyboard	A short white keyboard
A short tree	A tall green tree	A toy bus	One decker toy bus
A blue bicycle	A black bicycle	A blue chair	A wooden chair
A red kite	A long blue kite	A TV remote	A long white remote
A book with blue cover	A black book	Brown couch	A long brown couch
A open laptop	A black laptop	An egg sandwich	A meat sandwich
A cute toy train	A short blue toy train	Chocolate donut	Big circular donut

Kalyan Vasudev Alwala, Abhinav Gupta, and Shubham Tulsiani. Pre-train, self-train, distill: A simple recipe for supersizing 3d reconstruction. *CVPR*, 2022.

Jonathan T Barron, Ben Mildenhall, Matthew Tancik, Peter Hedman, Ricardo Martin-Brualla, and Pratul P Srinivasan. Mip-NeRF: A multiscale representation for anti-aliasing neural radiance fields. In *ICCV*, 2021.

Angel X. Chang, Thomas Funkhouser, Leonidas J. Guibas, Pat Hanrahan, Qixing Huang, Zimo Li, Silvio Savarese, Manolis Savva, Shuran Song, Hao Su, Jianxiong Xiao, Li Yi, and Fisher Yu. ShapeNet: An Information-Rich 3D Model Repository. Technical Report arXiv:1512.03012 [cs.GR], 2015.

Kevin Chen, Christopher B Choy, Manolis Savva, Angel X Chang, Thomas Funkhouser, and Silvio Savarese. Text2shape: Generating shapes from natural language by learning joint embeddings. In *ACCV*, 2018.

Zhiqin Chen and Hao Zhang. Learning implicit fields for generative shape modeling. In *CVPR*, 2019.

Ming Ding, Zhuoyi Yang, Wenyi Hong, Wendi Zheng, Chang Zhou, Da Yin, Junyang Lin, Xu Zou, Zhou Shao, Hongxia Yang, et al. Cogview: Mastering text-to-image generation via transformers. *NeurIPS*, 2021.

Jun Gao, Tianchang Shen, Zian Wang, Wenzheng Chen, Kangxue Yin, Daiqing Li, Or Litany, Zan Gojcic, and Sanja Fidler. Get3d: A generative model of high quality 3d textured shapes learned from images. *NeurIPS*, 2022.

Martin Heusel, Hubert Ramsauer, Thomas Unterthiner, Bernhard Nessler, and Sepp Hochreiter. GANs trained by a two time-scale update rule converge to a local Nash equilibrium. *NIPS*, 2017.

Fangzhou Hong, Mingyuan Zhang, Liang Pan, Zhongang Cai, Lei Yang, and Ziwei Liu. Avatarclip: Zero-shot text-driven generation and animation of 3d avatars. *ACM TOG (SIGGRAPH)*, 2022.

Tansin Jahan, Yanran Guan, and Oliver van Kaick. Semantics-guided latent space exploration for shape generation. In *COMPUT GRAPH FORUM*, 2021.

Ajay Jain, Matthew Tancik, and Pieter Abbeel. Putting nerf on a diet: Semantically consistent few-shot view synthesis. In *ICCV*, 2021.

Ajay Jain, Ben Mildenhall, Jonathan T Barron, Pieter Abbeel, and Ben Poole. Zero-shot text-guided object generation with drefam fields. In *CVPR*, 2022.

-
- Nikolay Jetchev. ClipMatrix: Text-controlled creation of 3d textured meshes. *arXiv preprint arXiv:2109.12922*, 2021.
- Bowen Li, Xiaojuan Qi, Thomas Lukasiewicz, and Philip H. S. Torr. Controllable text-to-image generation. *NeurIPS*, 2019.
- Bowen Li, Xiaojuan Qi, Thomas Lukasiewicz, and Philip H. S. Torr. ManiGAN: Text-guided image manipulation. In *CVPR*, 2020.
- Juncheng Li, Xin He, Longhui Wei, Long Qian, Linchao Zhu, Lingxi Xie, Yueting Zhuang, Qi Tian, and Siliang Tang. Fine-grained semantically aligned vision-language pre-training. *arXiv preprint arXiv:2208.02515*, 2022.
- Weixin Liang, Yuhui Zhang, Yongchan Kwon, Serena Yeung, and James Zou. Mind the gap: Understanding the modality gap in multi-modal contrastive representation learning. *arXiv preprint arXiv:2203.02053*, 2022.
- Xingchao Liu, Chengyue Gong, Lemeng Wu, Shujian Zhang, Hao Su, and Qiang Liu. FuseDream: Training-free text-to-image generation with improved CLIP+ GAN space optimization. *arXiv preprint arXiv:2112.01573*, 2021.
- Zhengzhe Liu, Yi Wang, Xiaojuan Qi, and Chi-Wing Fu. Towards implicit text-guided 3d shape generation. In *CVPR*, 2022.
- Oscar Michel, Roi Bar-On, Richard Liu, Sagie Benaim, and Rana Hanocka. Text2mesh: Text-driven neural stylization for meshes. In *CVPR*, 2022.
- Ben Mildenhall, Pratul P Srinivasan, Matthew Tancik, Jonathan T Barron, Ravi Ramamoorthi, and Ren Ng. NeRF: Representing scenes as neural radiance fields for view synthesis. In *ECCV*, 2020.
- Jacob Munkberg, Jon Hasselgren, Tianchang Shen, Jun Gao, Wenzheng Chen, Alex Evans, Thomas Müller, and Sanja Fidler. Extracting triangular 3d models, materials, and lighting from images. In *CVPR*, 2022.
- Alex Nichol, Prafulla Dhariwal, Aditya Ramesh, Pranav Shyam, Pamela Mishkin, Bob McGrew, Ilya Sutskever, and Mark Chen. GLIDE: Towards photorealistic image generation and editing with text-guided diffusion models. *arXiv preprint arXiv:2112.10741*, 2021.
- Michael Niemeyer, Lars Mescheder, Michael Oechsle, and Andreas Geiger. Differentiable volumetric rendering: Learning implicit 3D representations without 3D supervision. In *CVPR*, 2020.
- Adam Paszke, Sam Gross, Francisco Massa, Adam Lerer, James Bradbury, Gregory Chanan, Trevor Killeen, Zeming Lin, Natalia Gimelshein, Luca Antiga, et al. PyTorch: An imperative style, high-performance deep learning library. *NeurIPS*, 2019.
- Or Patashnik, Zongze Wu, Eli Shechtman, Daniel Cohen-Or, and Dani Lischinski. StyleCLIP: Text-driven manipulation of StyleGAN imagery. *ICCV*, 2021.
- Tingting Qiao, Jing Zhang, Duanqing Xu, and Dacheng Tao. MirrorGAN: Learning text-to-image generation by redescription. In *CVPR*, 2019.
- Alec Radford, Jong Wook Kim, Chris Hallacy, Aditya Ramesh, Gabriel Goh, Sandhini Agarwal, Girish Sastry, Amanda Askell, Pamela Mishkin, Jack Clark, et al. Learning transferable visual models from natural language supervision. In *ICML*, 2021.
- Aditya Ramesh, Mikhail Pavlov, Gabriel Goh, Scott Gray, Chelsea Voss, Alec Radford, Mark Chen, and Ilya Sutskever. Zero-shot text-to-image generation. In *ICML*, 2021.
- Aditya Ramesh, Prafulla Dhariwal, Alex Nichol, Casey Chu, and Mark Chen. Hierarchical text-conditional image generation with CLIP latents. *arXiv preprint arXiv:2204.06125*, 2022.
- Scott Reed, Zeynep Akata, Xinchen Yan, Lajanugen Logeswaran, Bernt Schiele, and Honglak Lee. Generative adversarial text to image synthesis. In *ICML*, 2016a.

-
- Scott E. Reed, Zeynep Akata, Santosh Mohan, Samuel Tenka, Bernt Schiele, and Honglak Lee. Learning what and where to draw. *NIPS*, 2016b.
- Jeremy Reizenstein, Roman Shapovalov, Philipp Henzler, Luca Sbordone, Patrick Labatut, and David Novotny. Common objects in 3D: Large-scale learning and evaluation of real-life 3D category reconstruction. In *ICCV*, 2021.
- Robin Rombach, Patrick Esser, and Björn Ommer. Network-to-network translation with conditional invertible neural networks. *NeurIPS*, 2020.
- Aditya Sanghi, Hang Chu, Joseph G Lambourne, Ye Wang, Chin-Yi Cheng, and Marco Fumero. CLIP-Forge: Towards zero-shot text-to-shape generation. In *CVPR*, 2022.
- Douglas M. Souza, Jônatas Wehrmann, and Duncan D. Ruiz. Efficient neural architecture for text-to-image synthesis. In *IJCNN*, 2020.
- David Stap, Maurits Bleeker, Sarah Ibrahimi, and Maartje ter Hoeve. Conditional image generation and manipulation for user-specified content. *CVPRW*, 2020.
- Can Wang, Menglei Chai, Mingming He, Dongdong Chen, and Jing Liao. CLIP-NeRF: Text-and-image driven manipulation of neural radiance fields. In *CVPR*, 2022a.
- Hao Wang, Guosheng Lin, Steven Hoi, and Chunyan Miao. Cycle-consistent inverse GAN for text-to-image synthesis. *ACM MM*, 2021.
- Zihao Wang, Wei Liu, Qian He, Xinglong Wu, and Zili Yi. CLIP-GEN: Language-free training of a text-to-image generator with CLIP. In *arXiv preprint arXiv:2203.00386*, 2022b.
- Zixu Wang, Zhe Quan, Zhi-Jie Wang, Xinjian Hu, and Yangyang Chen. Text to image synthesis with bidirectional generative adversarial network. In *ICME*, 2020.
- Weihao Xia, Yujia Yang, Jing-Hao Xue, and Baoyuan Wu. TediGAN: Text-guided diverse face image generation and manipulation. In *CVPR*, 2021.
- Tao Xu, Pengchuan Zhang, Qiuyuan Huang, Han Zhang, Zhe Gan, Xiaolei Huang, and Xiaodong He. AttnGAN: Fine-grained text to image generation with attentional generative adversarial networks. In *CVPR*, 2018.
- Lewei Yao, Runhui Huang, Lu Hou, Guansong Lu, Minzhe Niu, Hang Xu, Xiaodan Liang, Zhenguo Li, Xin Jiang, and Chunjing Xu. Filip: Fine-grained interactive language-image pre-training. *ICLR*, 2022.
- Mingkuan Yuan and Yuxin Peng. Bridge-GAN: Interpretable representation learning for text-to-image synthesis. *IEEE TCSVT*, 2019.
- Han Zhang, Tao Xu, Hongsheng Li, Shaoting Zhang, Xiaogang Wang, Xiaolei Huang, and Dimitris N. Metaxas. StackGAN: Text to photo-realistic image synthesis with stacked generative adversarial networks. In *ICCV*, 2017.
- Han Zhang, Tao Xu, Hongsheng Li, Shaoting Zhang, Xiaogang Wang, Xiaolei Huang, and Dimitris N. Metaxas. StackGAN++: Realistic image synthesis with stacked generative adversarial networks. *IEEE TPAMI*, 2018.
- Yufan Zhou, Ruiyi Zhang, Changyou Chen, Chunyuan Li, Chris Tensmeyer, Tong Yu, Jiuxiang Gu, Jinhui Xu, and Tong Sun. LAFITE: Towards language-free training for text-to-image generation. In *CVPR*, 2022.
- Nikola Zubić and Pietro Liò. An effective loss function for generating 3D models from single 2D image without rendering. *arXiv preprint arXiv:2103.03390*, 2021.